Nano Research 2015, 8(11): 3662–3672
DOI 10.1007/s12274-015-0866-z
Research Article
ISSN 1998-0124
CN 11-5974/O4

A universal etching-free transfer of MoS_2 films for applications in photodetectors

Donglin Ma[1], Jianping Shi[1,2], Qingqing Ji[1], Ke Chen[1], Jianbo Yin[1], Yuanwei Lin[1], Yu Zhang[1,2], Mengxi Liu[1], Qingliang Feng[1], Xiuju Song[1], Xuefeng Guo[1], Jin Zhang[1], Yanfeng Zhang[1,2] (✉), and Zhongfan Liu[1] (✉)

[1] *Department of Physical Chemistry, College of Chemistry and Molecular Engineering, Peking University, Beijing 100871, China*
[2] *Department of Materials Science and Engineering, College of Engineering, Peking University, Beijing 100871, China*

Received: 13 May 2015
Revised: 15 July 2015
Accepted: 22 July 2015

KEYWORDS
MoS_2,
etching-free,
efficient transfer,
ultrasonic bubbling,
environmental friendliness

ABSTRACT

Transferring MoS_2 films from growth substrates onto target substrates is a critical issue for their practical applications. Moreover, it remains a great challenge to avoid sample degradation and substrate destruction, because the current transfer method inevitably employs a wet chemical etching process. We developed an etching-free transfer method for transferring MoS_2 films onto arbitrary substrates by using ultrasonication. Briefly, the collapse of ultrasonication-generated microbubbles at the interface between polymer-coated MoS_2 film and substrates induce sufficient force to delaminate the MoS_2 films. Using this method, the MoS_2 films can be transferred from all substrates (silica, mica, strontium titanate, and sapphire) and retains the original sample morphology and quality. This method guarantees a simple transfer process and allows the reuse of growth substrates, without involving any hazardous etchants. The etching-free transfer method is likely to promote broad applications of MoS_2 in photodetectors.

1 Introduction

In recent years, atomically thin two-dimensional layered transition metal dichalcogenides (TMDCs) have attracted tremendous attention due to their intriguing electronic and optical properties [1–6]. One of the widely investigated compounds, monolayer molybdenum disulfide (MoS_2), possesses unique properties of tunable bandgap [7, 8], strong light–matter interaction [9], and strong spin–orbit coupling [10]. These properties make MoS_2 complementary to graphene [11, 12], and therefore a perfect candidate for engineering a broad range of applications in field-effect transistors [13–18], photodetectors [19–21], and future spintronics and valleytronics [22–25].

Compared to the methods of mechanical exfoliation [13, 26], liquid exfoliation [27–29], and solvothermal synthesis [30], chemical vapor deposition (CVD) [31–44] has been proved to be the most effective route to synthesize millimeter-scale uniform monolayer MoS_2 on various substrates such as SiO_2 on Si (SiO_2/Si) [32, 40–42], mica [38], strontium titanate (STO) [37],

Address correspondence to Yanfeng Zhang, yanfengzhang@pku.edu.cn; Zhongfan Liu, zfliu@pku.edu.cn

and sapphire [35, 39, 43, 44]. However, a major challenge is transferring CVD-grown MoS_2 onto target substrates for characterization and further device fabrication while maintaining high fidelity, keeping both the morphological and physicochemical properties intact. Currently, the most widely adopted MoS_2 transfer is a wet-etching transfer method in which polymethyl methacrylate (PMMA) is coated onto the MoS_2 as a film support, and the composite stack is separated from the substrate using chemical etching. In this transfer process, which is in part an imitation of the transfer of graphene [45–48], chemical etching of the substrate [31, 40, 41, 49] is inevitably involved that leads to degraded film quality as well as damage to or even consumption of the substrate. Particularly, in the etching of substrates for MoS_2 growth, treatments using hydrogen fluoride (HF) or strong alkali, which are harsher than the graphene etching treatments using iron chloride ($FeCl_3$) [46] or ammonium persulfate ($(NH_4)_2S_2O_8$) [48], present a more severe corrosive hazard. In light of these factors, it would be of great value to develop a "green" transfer method with high fidelity, high efficiency, recyclable use of substrates, and increased environmental friendliness [49, 50].

In this paper, a facile and etching-free transfer method is described for transferring MoS_2 from currently used insulating growth substrates to target substrates. This method is aided by an ultrasonic process, which generates millions of micron-sized cavitation bubbles. The collapse of these bubbles produces sufficient force in the interface between the PMMA-capped MoS_2 and the substrate to drive overlayer delamination. This transfer method, referred to as "ultrasonic bubbling transfer", is free of any chemical etchant, and thus works as a physical exfoliation process. Because it introduces no hazardous pollutants to the environment, it can be seen as a "green" alternative to traditional chemical etching. The crystal quality of the as-grown film can be maintained to a large extent, which makes it possible to investigate various properties of the transferred MoS_2. Additionally, perfect preservation of the planeness of the growth substrate means that the substrate can be reused for more growth cycles, thus dramatically reducing both waste and the production cost.

2 Results and discussion

Figure 1(a) shows a schematic illustration of the ultrasonic process used to detach a PMMA/MoS_2 stack from the growth substrate. A typical bubbling cycle is presented in the right panel of Fig. 1(a), with the middle sine curve showing the pressure change as a function of ultrasonication time. Under an ultrasonic cycle, millions of cavitation bubbles are generated at the initial stage of the negative-pressure period of the ultrasonic wave (stage 1), and these bubbles rapidly expand into larger bubbles until the pressure suddenly switches from negative to positive (stage 2). In a short time, these bubbles are compressed and collapse at the rising of the positive-pressure period (stage 3), releasing an enormous amount of energy, which produces considerable force in the interface between the PMMA/MoS_2 stack and the insulating substrate. Over many bubbling cycles (stage 4), the bubbling-induced force steadily delaminates the PMMA/MoS_2 stack from the growth substrate. The ease of separation of the MoS_2 and substrate is possibly due to a weak adhesion in their interface, which should be caused by the easy water penetration into the interface arising from the hydrophilic nature of most of the growth substrates (mica, STO, sapphire, etc.). It is worth noting that, the interface of PMMA and MoS_2 is quite stable under the ultrasonication process, which is probably due to a relatively strong interface adhesion, arising from the relatively dense contact and similar hydrophobic nature of PMMA and MoS_2, as proposed by a recently published report [50].

Figure 1(b) illustrates the key steps in the transfer process. As-grown MoS_2 on the growth substrate (SiO_2/Si, mica, STO, or sapphire) is first spin-coated with PMMA (950K, ALLRESIST, AR-P 679.04) at a relatively low speed of 1,000 rpm to yield a PMMA film with a thickness of 0.3 μm. The film was annealed at 180 °C for 15 min to completely remove the residual solvent. The PMMA/MoS_2/substrate stack is then immersed in a beaker of water kept in an ultrasonic cleaner at 80 °C under a power of 180 W (fixed working frequency: 40 kHz, SB-3200 DTDN, Ningbo Scientz Biotech. Co., Ltd.) (Fig. 1(c)). Within a few seconds, the edge of the PMMA/MoS_2 film can be seen detaching from the substrate, eventually causing the PMMA/MoS_2

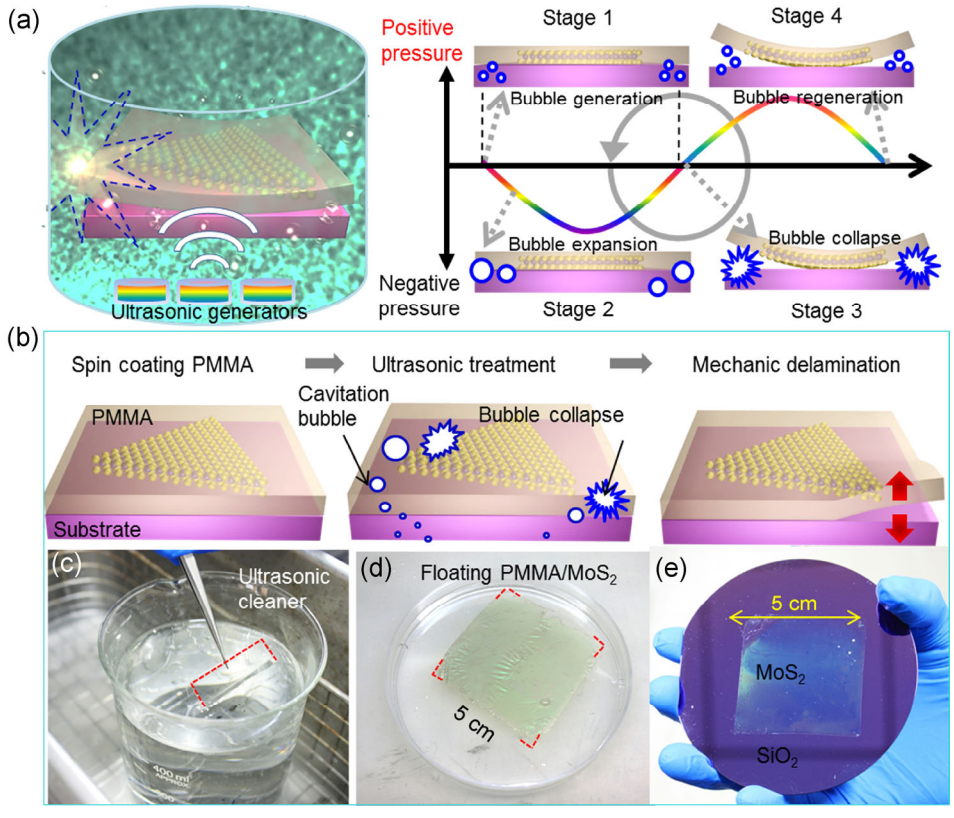

Figure 1 Illustration of ultrasonic bubbling transfer of MoS_2. (a) Schematics and principles of PMMA/MoS_2 stack delamination from the growth substrate. (b) Strategy for the ultrasonic bubbling transfer of MoS_2 on insulating substrates. (c) PMMA/MoS_2/mica stack immersed in a beaker of water kept in an ultrasonic cleaner. (d) 5 cm × 5 cm PMMA/MoS_2 stack floating on water. (e) Large-area transfer of MoS_2 onto arbitrary substrates like SiO_2/Si.

stack to float on the water surface (Fig. 1(d)). The delaminated PMMA/MoS_2 films can then be transferred onto any target substrate (such as SiO_2, Fig. 1(e)). Once the film is deposited on the target substrate, the PMMA can then be removed using acetone, which is the same process as the one used in graphene transfer. Notably, the entire delamination process uses only water and involves no chemical etchants or hazardous pollutants.

To demonstrate the universality of our transfer method, MoS_2 films were synthesized on SiO_2/Si, mica, STO, and sapphire growth substrates, and transferred to a target SiO_2/Si substrate. Different growth methods were also adopted. The sample grown on SiO_2/Si substrate was prepared by physical vapor deposition (PVD) [51] while the rest were grown by CVD. Different growth substrates were selected because they provide variable film coverage, from submonolayer to monolayer and even multilayer (> 4 layers), and variable MoS_2-flake shapes, from individual triangular islands to merged films. These variations are shown in the scanning electron microscopy (SEM) images in Figs. 2(a)–2(d). As shown in Figs. 2(e)–2(h), purple contrasts with the same dimensions as the growth substrates are clearly seen after the samples were transferred onto SiO_2/Si target substrates. The non-uniform coverage of the MoS_2 film grown on SiO_2/Si transferred to the target substrate (Fig. 1(e)) arises from the uneven growth of MoS_2 on SiO_2 in the PVD growth process (Fig. S1 in the Electronic Supplementary Material (ESM)). Corresponding optical microscopy (OM) images (Figs. 2(i)–2(l)) of the transferred samples, which are shown on a comparable length scale to the SEM images, display a perfect preservation of the coverage and morphology of the MoS_2 films throughout the ultrasonic bubbling transfer process (corresponding SEM data shown in Fig. S2 in the ESM). Corresponding Raman characterizations show frequency differences

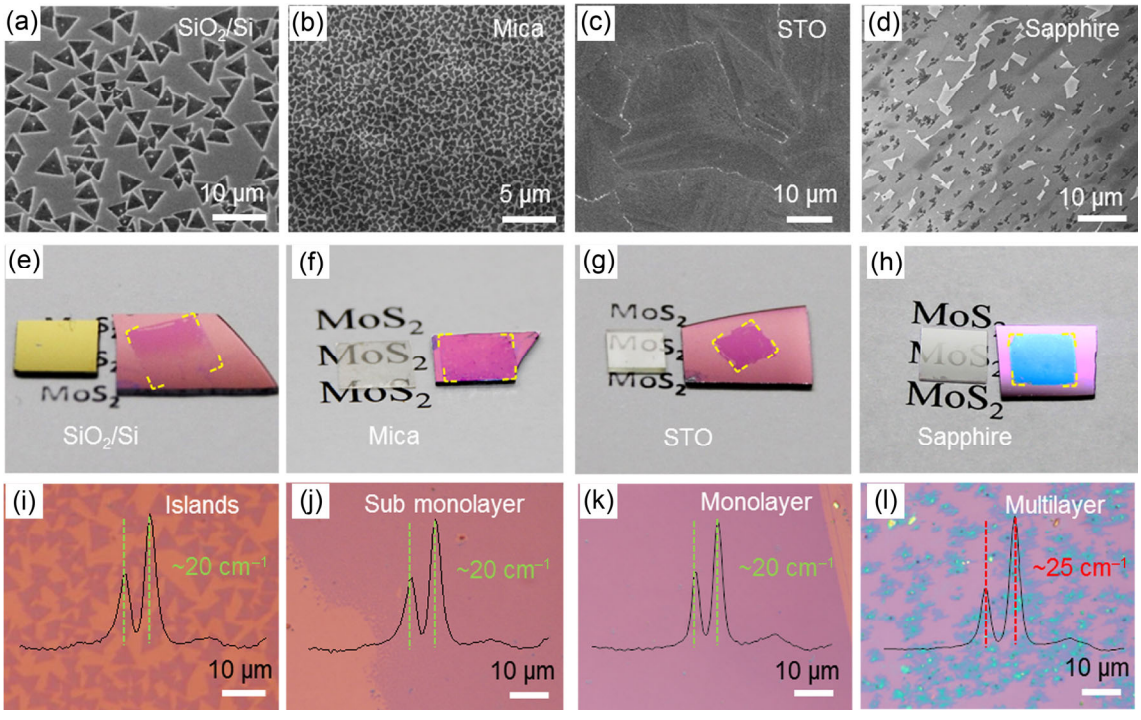

Figure 2 Universal transfer of MoS_2 grown on SiO_2/Si ((a), (e) and (i)), mica ((b), (f) and (j)), STO ((c), (g), and (k)) and sapphire ((d), (h) and (l)). (a)–(d) SEM images of as-grown MoS_2 on corresponding insulating substrates. (e)–(h) Photographs of the insulating substrates after sample transfer (left) and MoS_2 transferred onto SiO_2/Si target substrates (right). (i)–(l) OM images of MoS_2 transferred onto SiO_2/Si target substrates corresponding to (e)–(h), respectively. The overlaid spectra are corresponding Raman characterizations of the layer numbers ((i)–(k) for monolayer, and (l) multilayer in the deep contrast regions).

of 20 and 25 cm^{-1} between the two main peaks in the spectrum (corresponding to Raman modes of E^1_{2g}, A_{1g}), which correspond to the monolayer and multilayer films, respectively [52].

These results indicate that the ultrasonic bubbling transfer method can be widely used to transfer MoS_2 films synthesized on various substrates with perfect preservation of the coverage, morphology, and thickness of the MoS_2 film. It is noteworthy that this method is also effective in transferring WS_2 [53], another widely used TMDC (Fig. S3 in the ESM), which suggests that it could be applied to many other TMDCs.

In addition to preservation of the film morphology, preservation of the crystal quality is an essential parameter for evaluating a transfer method. Figure 3(a) shows the characterization of a monolayer MoS_2 film grown on sapphire and transferred onto a Si/SiO_2 target substrate. The photographs show a uniform color contrast within a sample size of around 1 cm × 1 cm. A series of OM images (Figs. 3(b)–3(d)) were captured in sequence from the left boundary to the inner part of the transferred film, covering a total length of 4.5 mm. Uniform and continuous contrasts can be clearly seen, dispelling the concern that the bubbling process may have caused mechanical damage to the transferred MoS_2 films. In order to confirm the high fidelity of the crystal quality, Raman (from 370 to 420 cm^{-1}) and PL mappings (from 640 to 670 nm) were obtained for a monolayer film and a triangular island (OM images shown in Figs. 3(e) and 3(h)), respectively. These results show uniform contrasts in the mapped regions (Figs. 3(f), 3(i), 3(g), and 3(j)), which are indicative of uniform crystal quality. Meanwhile, single-point Raman spectra of the transferred samples (Fig. 3(k)) exhibit two typical peaks, with the in-plane vibration of Mo and S atoms (E^1_{2g}) at ~385 cm^{-1} and the out-of-plane vibration of S atoms (A_{1g}) at ~405 cm^{-1}, with a frequency difference of ~20 cm^{-1}, which are in line with the Raman spectra of the pristine monolayer MoS_2 on the sapphire growth substrate. Moreover, single-point PL spectra (Fig. 3(l)) show the intense characteristic peak of an excitonic emission at 662 nm

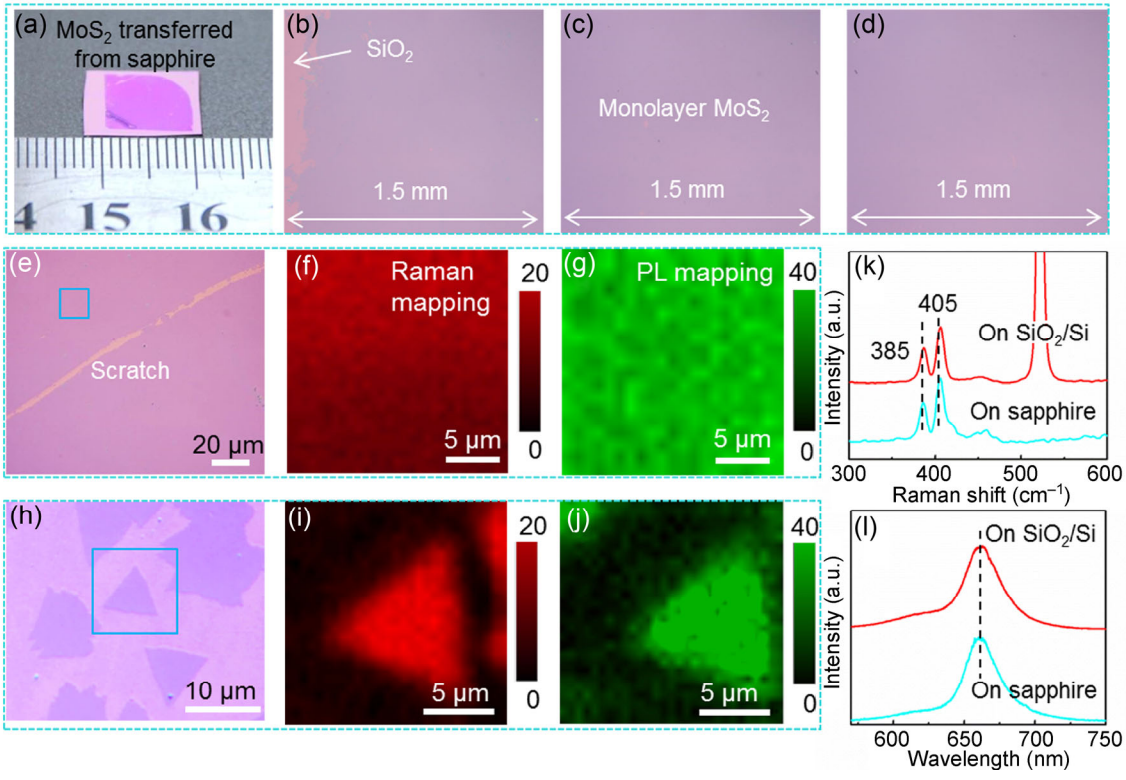

Figure 3 Large-scale OM and Raman characterizations of MoS_2 transferred onto SiO_2/Si. (a) Photograph showing the centimeter-scale uniform transfer of a monolayer MoS_2 film grown on sapphire onto a Si/SiO_2 substrate. (b)–(d) Sequential OM images of sample (a) captured from the left boundary to the inner part of the sample showing a uniform color contrast. (e) and (h) OM images of a monolayer film consisting of a scratch line and submonolayer triangular MoS_2 flakes, respectively. (f) and (i) Corresponding Raman mapping of the area marked by squares in (e) and (h), respectively. (g) and (j) PL mapping of the same areas of (f) and (i) showing uniform color contrasts over the MoS_2-covered regions, indicative of almost no crystal quality degradation through the transfer process. (k) and (l) Raman and PL spectra collected from randomly chosen locations on the monolayer MoS_2 on the sapphire growth substrate and Si/SiO_2 target substrate.

for both the pristine and transferred MoS_2 samples, again suggesting perfect preservation of the high crystal quality. A quality survey of transferred MoS_2 samples grown on the other three substrates is provided in Fig. S4 in the ESM. These spectroscopy measurements indicate that all the transferred MoS_2 samples retain their pre-transfer properties. Of special note here is that by using this newly developed ultrasonic bubbling transfer method, the crystal quality of the transferred samples should be at least comparable to that obtained using the wet chemical etching method (comparison of different transfer methods shown in Fig. S5 in the ESM).

A significant advantage of this ultrasonic bubbling transfer method is that it can be utilized to prepare clean samples for transmission electron microscopy (TEM) characterization. The optical image in Fig. 4(a) shows several triangle-shaped flakes of MoS_2 transferred onto a carbon-film-coated Cu grid. The morphology of the triangular MoS_2 flakes is well preserved through the transfer process. A typical triangular MoS_2 island with sharp edges is shown in Fig. 4(b), with corresponding selected area electron diffraction (SAED) (Fig. 4(c)) showing diffraction spots with six-fold symmetry. This is highly suggestive of a single-crystal sample. In a detailed study, the diffraction spots in six-fold symmetry could be further divided into two sets of spots with three-fold symmetry, corresponding to the Mo and S sublattices. According to the line profile along the white dashed line (Fig. 4(c) overlay), $\boldsymbol{k}_a$ with higher intensity refers to the Mo sublattice with respect to $\boldsymbol{k}_b$ with lower intensity in parallel with the S sublattice [40]. The relative intensities of $\boldsymbol{k}_a$ and $\boldsymbol{k}_b$ can be utilized to identify the Mo-terminated

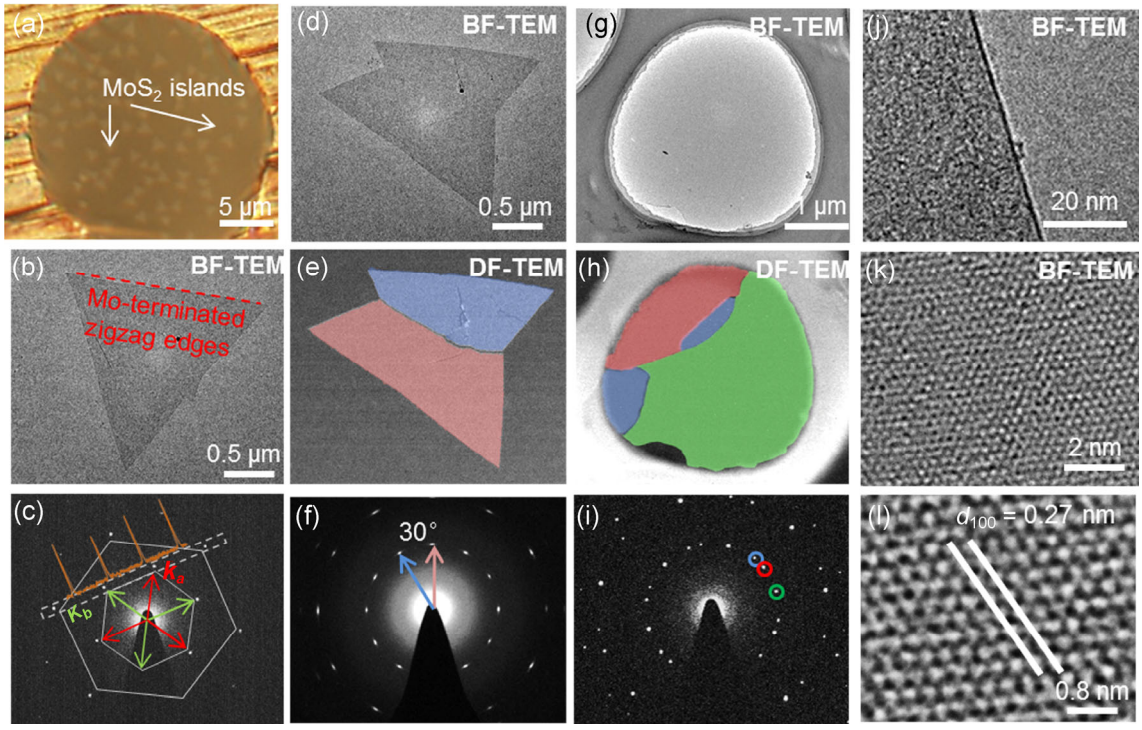

Figure 4 Transferability of MoS_2 onto TEM grids via the ultrasonic bubbling transfer method. (a) Optical image of multiple MoS_2 islands transferred onto carbon-film-coated Cu grids. (b) BF-TEM image of a MoS_2 triangle showing a Mo zigzag edge orientation, as confirmed by the corresponding SAED pattern shown in (c). The asymmetry of Mo and S sublattices divides the hexagonal diffraction spots into two families: $\boldsymbol{k}_a$ and $\boldsymbol{k}_b$. Overlaid is a line profile that was scanned along the white dashed line. The higher intensity $\boldsymbol{k}_a$ spots correspond to the Mo sublattice, as indicated by red arrows in (b). (d) BF-TEM image of a polycrystalline MoS_2 flake created by two merged triangular flakes. (e) False-color DF-TEM image corresponding to two sets of diffraction patterns in (f). (f) Diffraction pattern of the MoS_2 flake in (d); two sets of diffraction patterns are indicated by blue and pink arrows, respectively. (g) BF-TEM image of a continuous monolayer MoS_2 film transferred onto a lacey carbon-film-coated Cu TEM grid. (h) False-color DF-TEM image corresponding to the three sets of diffraction patterns in (i). (j) Cross-section TEM image on the film edge. (k) and (l) Atomically resolved TEM images of monolayer MoS_2.

zigzag edge of a MoS_2 triangular flake (TEM image of single-crystal MoS_2 islands with S-terminated edges in Fig. S6 in the ESM). Besides single-crystalline triangles, polycrystalline MoS_2 flakes formed by the aggregation of more than one triangle can also be perfectly transferred onto carbon-film-coated Cu grids. For example, Fig. 4(d) shows the bright field TEM (BF-TEM) image of a typical polygonal-shaped MoS_2 island. The corresponding false-color dark field TEM (DF-TEM) image and SAED pattern in Figs. 4(e) and 4(f) can be utilized to identify the domain boundary and to observe a relative rotation of ~30° between the two composite domains.

In addition, as shown in Fig. 4(g), a uniform monolayer MoS_2 film was transferred intact onto a lacey carbon-film-coated Cu grid, as evidenced by a freestanding MoS_2 film residing on a hole with a diameter of ~4 μm. In accordance with the diffraction spots in Fig. 4(i), the false-color DF-TEM image in Fig. 4(h) marks the different orientations of the MoS_2 domains with different colors. Moreover, a cross-section TEM image taken at the edge of the MoS_2 film shows only one dark-line contrast. This provides solid proof that the transferred film is monolayer. Of particular significance is the fact that high-resolution TEM images in Figs. 4(k) and 4(l) exhibit perfect atomic lattices with hexagonal symmetry extending over tens of nanometers. The d(100) distance, as marked by two parallel white lines in Fig. 4(l), is measured to be around 0.27 nm, which is in agreement with the lattice constant of MoS_2. Therefore, the developed physical transfer method is qualified for

improved TEM characterization of MoS_2 and similar materials.

Another important aspect of evaluating a transfer method is determining its ability to preserve the growth substrate for reuse. As the ultrasonic bubbling transfer method is similar to physical exfoliation, it is likely that recycling would be possible. Figure 5(a) presents the surviving sapphire substrates from bubbling transfer (1) and chemical etching transfer (2). It is evident in the photographs that substrate 1 has retained its smooth surface, which indicates that the pristine sapphire single crystal has not been damaged. In contrast, substrate 2 appears to have a very rough surface. Substrate 1 was further characterized by atomic force microscopy (AFM), which showed the surface to be quite clean and free of any defects or residue. This qualifies the recycle use of sapphire substrates for repetitive MoS_2 growth (Fig. 5(b)). Interestingly, triangular MoS_2 flakes can be successfully grown on substrate 1 by CVD method with same conditions, even after several transfers using ultrasonic bubbling (Fig. 5(c)). The grown flakes are similar to those produced on a sapphire substrate in the first round (Fig. S7(a) in the ESM). In contrast, substrate 2 was unclean and rough after chemical etching and was decorated by irregular-shaped residues of MoS_2 or MoO_3 particles (Figs. S7(b) and S7(c) in the ESM), rendering it unsuitable for reuse. In addition to preserving the growth substrate for reuse, a significant advantage of the ultrasonic bubbling transfer method is that the delamination process is very fast, taking on an average less than 1 min to complete, which significantly improves the efficiency of transfer. The chemical etching process, on the other hand, takes more than 30 min to completely delaminate a PMMA/MoS_2 stack from the growth substrate, as determined

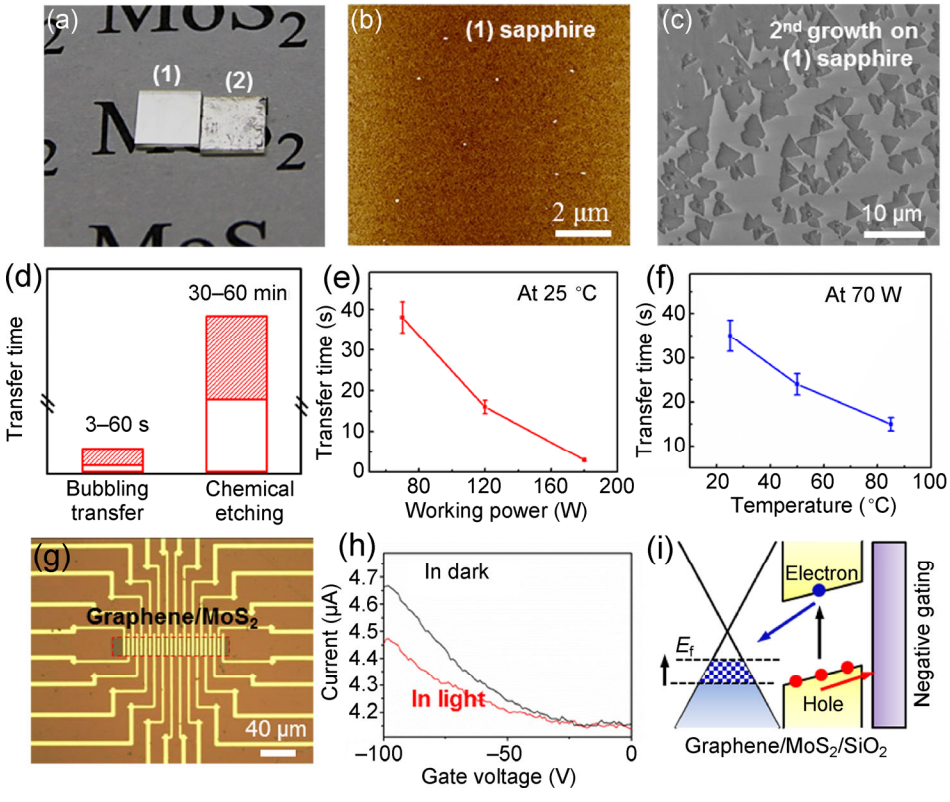

Figure 5 Demonstration of recycle use of growth substrates and graphene/MoS_2 nanodevice. (a) Photograph of sapphire substrates after ultrasonic bubbling transfer (1) and chemical etching transfer (2). (b) AFM image of (1) sapphire after ultrasonic bubbling transfer. (c) SEM image presenting the successful growth of MoS_2 on recycled sapphire (substrate 1) after several growth and transfer processes. (d) Efficiency comparison of ultrasonic bubbling and chemical etching transfer processes. (e) and (f) Effect of water temperature and working power of ultrasonication on transfer time. (g) Optical microscopy image of the graphene/MoS_2 layered heterostructure device. (h) *I*–*V* characteristics in the dark and in the presence of visible light. (i) Energy band diagram for the graphene/MoS_2 heterostructure.

from experimental statistics and reports in the published literature [54] (Fig. 5(d)).

Furthermore, the effect of water temperature and working power of ultrasonication on transfer time were also investigated. As shown in Fig. 5(e), at a relatively low ultrasonication power of 70 W, the increase of water temperature remarkably reduces the transfer time, from around 35 s at room temperature to around 15 s at 80 ℃. It is also not a surprise that the increase of ultrasonication power shortens the transfer time, from around 39 s at 70 W to merely 3 s at 180 W (maximum power of the equipment) (Fig. 5(f)). Based on these results, it can be inferred that the increase of water temperature and the working power of the ultrasonic equipment could enhance the ultrasonication cavitation and generate a stronger peeling force on the PMMA/MoS_2 stack, and finally induce a faster layer delamination.

In order to demonstrate the compatibility of this transfer method with nanodevice fabrication, a photodetector was prepared by stacking CVD monolayer graphene onto as-transferred MoS_2 on a 300-nm SiO_2/Si substrate (OM image shown in Fig. 5(g)). The source–drain current I versus back-gate voltage V characteristics of the graphene/MoS_2 device is presented in Fig. 5(h) in the dark and in the presence of visible light (a 150-W halogen lamp, light energy density of ~3 mW·cm^{-2}). It can be noticed that, both in the dark and light states, the source–drain current of the device increases with higher negative gate voltage. However, an obvious decrease of the current was observed when light was shed on the device channel, and the current drop increased with increased negative bias voltage (0.20 μA at –100 V). This phenomenon can be explained using the energy band diagram of the device (Fig. 5(i)). Under negative gate voltage, the photo-induced electrons from MoS_2 may be injected into graphene. This will raise the graphene Fermi level near the Dirac point, thus increasing the resistance, considering the hole-doped nature of CVD graphene [20]. In this regard, the photosensitivity of the device can be roughly estimated to be 1.3×10^4 A/W at a gate voltage of –100 V, which is much superior to the existing value for graphene [55] or single-layer MoS_2 [19] (performance of field-effect transistor devices shown in Fig. S8 in the ESM).

3 Conclusions

The ultrasonic bubbling transfer method developed in this study provides a novel "green" method for MoS_2 transfer. This method has been successfully applied to the four main growth substrates and can be extended to other systems. The etching-free transfer process is facile, fast, and totally "green" because it does not contaminate the MoS_2 samples and is environmentally friendly. Furthermore, this method preserves the surface of the growth substrate and enables its reuse for the growth of new MoS_2 films. This work can not only facilitate the characterization of the intrinsic properties of TMDCs, but also accelerate the potential application of MoS_2 in photodetectors.

4 Experimental

4.1 MoS_2 growth on SiO_2/Si, mica, STO, and sapphire substrates

MoS_2 was grown on a SiO_2/Si substrate according to the procedure described in Ref. [45]. For MoS_2 grown on mica, STO, and sapphire substrates, the growth was performed inside a tube furnace (Lindberg/Blue M) equipped with a 3-inch-diameter quartz tube. Sulfur powder (Alfa Aesar, purity 99.9%) was placed outside the hot zone and heated by heating belts to 135 ℃. MoO_3 powder (Alfa Aesar, purity 99.9%) and growth substrates (Hefei Kejing Material Technology Co., Ltd.) were sequentially placed inside the hot zone of the tube furnace. In a typical growth, argon gas at a rate of 50 sccm was used as the carrier gas, and the growth time was 1 h. More detailed growth parameters are described in Refs. [37, 38, 43, 44].

4.2 Characterization of transferred MoS_2

The MoS_2 samples were systematically characterized using optical microscopy (Olympus DX51), SEM (Hitachi S-4800; acceleration voltage of 1–2 kV), Raman spectroscopy (Horiba, LabRAM HR-800), TEM (JEOL JEM-2100F LaB6; acceleration voltage of 200 kV), ultraviolet-visible-infrared (UV-vis-IR) spectroscopy (Perkin-Elmer Lambda 950 spectrophotometer), AFM (Vecco Nanoscope III), and electrical measurements

(Keithley SCS-4200). The photodetector device was fabricated by photolithography and subsequent thermal evaporation of 8-nm Cr/60-nm Au contacts.

Acknowledgements

This work was financially supported by the National Natural Science Foundation of China (Nos. 51222201, 51290272, 51472008, and 51432002), the National Basic Research Program of China (Nos. 2012CB921404, 2013CB932603, 2012CB933404, and 2011CB921903), and the Foundation for Innovative Research Groups of the National Natural Science Foundation of China (No. 51121091).

Electronic Supplementary Material: Supplementary material (SEM images of PVD grown MoS_2 on SiO_2/Si, SEM images of MoS_2 transferred onto SiO_2/Si from different growth substrate, characterization of WS_2 transfer, Raman and PL spectra comparison of as-grown and transferred MoS_2, electronic measurement of MoS_2 based FET device) is available in the online version of this article at http://dx.doi.org/10.1007/s12274-015-0866-z.

References

[1] Chhowalla, M.; Shin, H. S.; Eda, G.; Li, L. J.; Loh, K. P.; Zhang, H. The chemistry of two-dimensional layered transition metal dichalcogenide nanosheets. *Nat. Chem.* **2013**, *5*, 263–275.

[2] Huang, X.; Zeng, Z. Y.; Zhang, H. Metal dichalcogenide nanosheets: Preparation, properties and applications. *Chem. Soc. Rev.* **2013**, *42*, 1934–1946.

[3] Wang, Q. H.; Kalantar-Zadeh, K.; Kis, A.; Coleman, J. N.; Strano, M. S. Electronics and optoelectronics of two-dimensional transition metal dichalcogenides. *Nat. Nanotechnol.* **2012**, *7*, 699–712.

[4] Yin, X. B.; Ye, Z. L.; Chenet, D. A.; Ye, Y.; O'Brien, K.; Hone, J. C.; Zhang, X. Edge nonlinear optics on a MoS_2 atomic monolayer. *Science* **2014**, *344*, 488–490.

[5] Mak, K. F.; He, K. L.; Lee, C.; Lee, G. H.; Hone, J.; Heinz, T. F.; Shan, J. Tightly bound trions in monolayer MoS_2. *Nat. Mater.* **2013**, *12*, 207–211.

[6] Li, H.; Wu, J.; Yin, Z. Y.; Zhang, H. Preparation and applications of mechanically exfoliated single-layer and multilayer MoS_2 and WSe_2 nanosheets. *Acc. Chem. Res.* **2014**, *47*, 1067–1075.

[7] Jin, W. C.; Yeh, P.-C.; Zaki, N.; Zhang, D. T.; Sadowski, J. T.; Al-Mahboob, A.; van der Zande, A. M.; Chenet, D. A.; Dadap, J. I.; Herman, I. P. et al. Direct measurement of the thickness-dependent electronic band structure of MoS_2 using angle-resolved photoemission spectroscopy. *Phys. Rev. Lett.* **2013**, *111*, 106801.

[8] Eknapakul, T.; King, P. D. C.; Asakawa, M.; Buaphet, P.; He, R. H.; Mo, S. K.; Takagi, H.; Shen, K. M.; Baumberger, F.; Sasagawa, T. et al. Electronic structure of a quasi-freestanding MoS_2 monolayer. *Nano Lett.* **2014**, *14*, 1312–1316.

[9] Britnell, L.; Ribeiro, R. M.; Eckmann, A.; Jalil, R.; Belle, B. D.; Mishchenko, A.; Kim, Y. J.; Gorbachev, R. V.; Georgiou, T.; Morozov, S. V. et al. Strong light-matter interactions in heterostructures of atomically thin films. *Science* **2013**, *340*, 1311–1314.

[10] Coehoorn, R.; Haas, C.; Dijkstra, J.; Flipse, C. J. F.; de Groot, R. A.; Wold, A. Electronic structure of $MoSe_2$, MoS_2, WSe_2. I. Band-structure calculations and photoelectron spectroscopy. *Phys. Rev. B* **1987**, *35*, 6195–6202.

[11] Novoselov, K. S.; Geim, A. K.; Morozov, S. V.; Jiang, D.; Zhang, Y.; Dubonos, S. V.; Grigorieva, I. V.; Firsov, A. A. Electric field effect in atomically thin carbon films. *Science* **2004**, *306*, 666–669.

[12] Novoselov, K. S.; Geim, A. K.; Morozov, S. V.; Jiang, D.; Katsnelson, M. I.; Grigorieva, I. V.; Dubonos, S. V.; Firsov, A. A. Two-dimensional gas of massless Dirac fermions in graphene. *Nature* **2005**, *438*, 197–200.

[13] Radisavljevic, B.; Radenovic, A.; Brivio, J.; Giacometti, V.; Kis, A. Single-layer MoS_2 transistors. *Nat. Nanotechnol.* **2011**, *6*, 147–150.

[14] Fuhrer, M. S.; Hone, J. Measurement of mobility in dual-gated MoS_2 transistors. *Nat. Nanotechnol.* **2013**, *8*, 146–147.

[15] Wang, H.; Yu, L. L.; Lee, Y.-H.; Shi, Y. M.; Hsu, A.; Chin, M. L.; Li, L.-J.; Dubey, M.; Kong, J.; Palacios, T. Integrated circuits based on bilayer MoS_2 transistors. *Nano Lett.* **2012**, *12*, 4674–4680.

[16] Yin, Z. Y.; Li, H.; Li, H.; Jiang, L.; Shi, Y. M.; Sun, Y. H.; Lu, G.; Zhang, Q.; Chen, X. D.; Zhang, H. Single-layer MoS_2 phototransistors. *ACS Nano* **2012**, *6*, 74–80.

[17] He, Q. Y.; Zeng, Z. Y.; Yin, Z. Y.; Li, H.; Wu, S. X.; Huang, X.; Zhang, H. Fabrication of flexible MoS_2 thin-film transistor arrays for practical gas-sensing applications. *Small* **2012**, *8*, 2994–2999.

[18] Li, H.; Yin, Z. Y.; He, Q. Y.; Li, H.; Huang, X.; Lu, G.; Fam, D. W. H.; Tok, A. I. Y.; Zhang, Q.; Zhang, H. Fabrication of single- and multilayer MoS_2 film-based field-effect transistors for sensing NO at room temperature. *Small* **2012**, *8*, 63–67.

[19] Lopez-Sanchez, O.; Lembke, D.; Kayci, M.; Radenovic, A.; Kis, A. Ultrasensitive photodetectors based on monolayer MoS_2. *Nat. Nanotechnol.* **2013**, *8*, 497–501.

[20] Roy, K.; Padmanabhan, M.; Goswami, S.; Sai, T. P.; Ramalingam, G.; Raghavan, S.; Ghosh, A. Graphene–MoS_2 hybrid structures for multifunctional photoresponsive memory devices. *Nat. Nanotechnol.* **2013**, *8*, 826–830.

[21] Bertolazzi, S.; Krasnozhon, D.; Kis, A. Nonvolatile memory cells based on MoS_2/graphene heterostructures. *ACS Nano* **2013**, *7*, 3246–3252.

[22] Mak, K. F.; He, K. L.; Shan, J.; Heinz, T. F. Control of valley polarization in monolayer MoS_2 by optical helicity. *Nat. Nanotechnol.* **2012**, *7*, 494–498.

[23] Mak, K. F.; McGill, K. L.; Park, J.; McEuen, P. L. The valley Hall effect in MoS_2 transistors. *Science* **2014**, *344*, 1489–1492.

[24] Zeng, H. L.; Dai, J. F.; Yao, W.; Xiao, D.; Cui, X. D. Valley polarization in MoS_2 monolayers by optical pumping. *Nat. Nanotechnol.* **2012**, *7*, 490–493.

[25] Wu, S. F.; Ross, J. S.; Liu, G.-B.; Aivazian, G.; Jones, A.; Fei, Z. Y.; Zhu, W. G.; Xiao, D.; Yao, W.; Cobden, D. et al. Electrical tuning of valley magnetic moment through symmetry control in bilayer MoS_2. *Nat. Phys.* **2013**, *9*, 149–153.

[26] Mak, K. F.; Lee, C.; Hone, J.; Shan, J.; Heinz, T. F. Atomically thin MoS_2: A new direct-gap semiconductor. *Phys. Rev. Lett.* **2010**, *105*, 136805.

[27] Coleman, J. N.; Lotya, M.; O'Neill, A.; Bergin, S. D.; King, P. J.; Khan, U.; Young, K.; Gaucher, A.; De, S.; Smith, R. J. et al. Two-dimensional nanosheets produced by liquid exfoliation of layered materials. *Science* **2011**, *331*, 568–571.

[28] Zeng, Z. Y.; Yin, Z. Y.; Huang, X.; Li, H.; He, Q. Y.; Lu, G.; Boey, F.; Zhang, H. Single-layer semiconducting nanosheets: High-yield preparation and device fabrication. *Angew. Chem., Int. Ed.* **2011**, *50*, 11093–11097.

[29] Zeng, Z. Y.; Sun, T.; Zhu, J. X.; Huang, X.; Yin, Z. Y.; Lu, G.; Fan, Z. X.; Yan, Q. Y.; Hng, H. H.; Zhang, H. An effective method for the fabrication of few-layer-thick inorganic nanosheets. *Angew. Chem., Int. Ed.* **2012**, *51*, 9052–9056.

[30] Li, Y. G.; Wang, H. L.; Xie, L. M.; Liang, Y. Y.; Hong, G. S.; Dai, H. J. MoS_2 nanoparticles grown on graphene: An advanced catalyst for the hydrogen evolution reaction. *J. Am. Chem. Soc.* **2011**, *133*, 7296–7299.

[31] Lee, Y.-H.; Yu, L. L.; Wang, H.; Fang, W. J.; Ling, X.; Shi, Y. M.; Lin, C.-T.; Huang, J.-K.; Chang, M.-T.; Chang, C.-S. et al. Synthesis and transfer of single-layer transition metal disulfides on diverse surfaces. *Nano Lett.* **2013**, *13*, 1852–1857.

[32] Lee, Y. H.; Zhang, X. Q.; Zhang, W. J.; Chang, M. T.; Lin, C. T.; Chang, K. D.; Yu, Y. C.; Wang, J. T. W.; Chang, C. S.; Li, L. J. et al. Synthesis of large-area MoS_2 atomic layers with chemical vapor deposition. *Adv. Mater.* **2012**, *24*, 2320–2325.

[33] Zhan, Y. J.; Liu, Z.; Najmaei, S.; Ajayan, P. M.; Lou, J. Large-area vapor-phase growth and characterization of MoS_2 atomic layers on a SiO_2 substrate. *Small* **2012**, *8*, 966–971.

[34] Wang, X. S.; Feng, H. B.; Wu, Y. M.; Jiao, L. Y. Controlled synthesis of highly crystalline MoS_2 flakes by chemical vapor deposition. *J. Am. Chem. Soc.* **2013**, *135*, 5304–5307.

[35] Liu, K.-K.; Zhang, W.; Lee, Y.-H.; Lin, Y.-C.; Chang, M.-T.; Su, C.-Y.; Chang, C.-S.; Li, H.; Shi, Y.; Zhang, H. et al. Growth of large-area and highly crystalline MoS_2 thin layers on insulating substrates. *Nano Lett.* **2012**, *12*, 1538–1544.

[36] Ling, X.; Lee, Y.-H.; Lin, Y. X.; Fang, W. J.; Yu, L. L.; Dresselhaus, M. S.; Kong, J. Role of the seeding promoter in MoS_2 growth by chemical vapor deposition. *Nano Lett.* **2014**, *14*, 464–472.

[37] Zhang, Y.; Ji, Q. Q.; Han, G. F.; Ju, J.; Shi, J. P.; Ma, D. L.; Sun, J. Y.; Zhang, Y. S.; Li, M. J.; Lang, X. Y. et al. Dendritic, transferable, strictly monolayer MoS_2 flakes synthesized on $SrTiO_3$ single crystals for efficient electrocatalytic applications. *ACS Nano* **2014**, *8*, 8617–8624.

[38] Ji, Q. Q.; Zhang, Y. F.; Gao, T.; Zhang, Y.; Ma, D. L.; Liu, M. X.; Chen, Y. B.; Qiao, X. F.; Tan, P.-H.; Kan, M. et al. Epitaxial monolayer MoS_2 on mica with novel photoluminescence. *Nano Lett.* **2013**, *13*, 3870–3877.

[39] Yu, Y. F.; Li, C.; Liu, Y.; Su, L. Q.; Zhang, Y.; Cao, L. Y. Controlled scalable synthesis of uniform, high-quality monolayer and few-layer MoS_2 films. *Sci. Rep.* **2013**, *3*, 1866.

[40] Najmaei, S.; Liu, Z.; Zhou, W.; Zou, X. L.; Shi, G.; Lei, S. D.; Yakobson, B. I.; Idrobo, J.-C.; Ajayan, P. M.; Lou, J. Vapour phase growth and grain boundary structure of molybdenum disulphide atomic layers. *Nat. Mater.* **2013**, *12*, 754–759.

[41] van der Zande, A. M.; Huang, P. Y.; Chenet, D. A.; Berkelbach, T. C.; You, Y. M.; Lee, G.-H.; Heinz, T. F.; Reichman, D. R.; Muller, D. A.; Hone, J. C. Grains and grain boundaries in highly crystalline monolayer molybdenum disulphide. *Nat. Mater.* **2013**, *12*, 554–561.

[42] Zhang, J.; Yu, H.; Chen, W.; Tian, X. Z.; Liu, D. H.; Cheng, M.; Xie, G. B.; Yang, W.; Yang, R.; Bai, X. D. et al. Scalable growth of high-quality polycrystalline MoS_2 monolayers on SiO_2 with tunable grain sizes. *ACS Nano* **2014**, *8*, 6024–6030.

[43] Dumcenco, D.; Ovchinnikov, D.; Marinov, K.; Lazić, P.; Gibertini, M.; Marzari, N.; Sanchez, O. L.; Kung, Y.-C.; Krasnozhon, D.; Chen, M.-W. et al. Large-area epitaxial monolayer MoS_2. *ACS Nano* **2015**, *9*, 4611–4620.

[44] Ji, Q. Q.; Kan, M.; Zhang, Y.; Guo, Y.; Ma, D. L.; Shi, J. P.; Sun, Q.; Chen, Q.; Zhang, Y. F.; Liu, Z. F. Unravelling orientation distribution and merging behavior of monolayer MoS_2 domains on sapphire. *Nano Lett.* **2015**, *15*, 198–205.

[45] Jiao, L. Y.; Fan, B.; Xian, X. J.; Wu, Z. Y.; Zhang, J.; Liu, Z. F. Creation of nanostructures with poly(methyl methacrylate)-mediated nanotransfer printing. *J. Am. Chem. Soc.* **2008**, *130*, 12612–12613.

[46] Reina, A.; Jia, X.; Ho, J.; Nezich, D.; Son, H.; Bulovic, V.; Dresselhaus, M. S.; Kong, J. Large area, few-layer graphene films on arbitrary substrates by chemical vapor deposition. *Nano Lett.* **2009**, *9*, 30–35.

[47] Bae, S.; Kim, H.; Lee, Y.; Xu, X. F.; Park, J.-S.; Zheng, Y.; Balakrishnan, J.; Lei, T.; Kim, H. R.; Song, Y. I. et al. Roll-to-roll production of 30-inch graphene films for transparent electrodes. *Nat. Nanotechnol.* **2010**, *5*, 574–578.

[48] Gao, L. B.; Ni, G.-X.; Liu, Y. P.; Liu, B.; Castro Neto, A. H.; Loh, K. P. Face-to-face transfer of wafer-scale graphene films. *Nature* **2014**, *505*, 190–194.

[49] Li, H.; Wu, J.; Huang, X.; Yin, Z. Y.; Liu, J. Q.; Zhang, H. A universal, rapid method for clean transfer of nanostructures onto various substrates. *ACS Nano* **2014**, *8*, 6563–6570.

[50] Gurarslan, A.; Yu, Y. F.; Su, L. Q.; Yu, Y. L.; Suarez, F.; Yao, S. S.; Zhu, Y.; Öztürk, M.; Zhang, Y.; Cao, L. Y. Surface energy-assisted perfect transfer of centimeter-scale monolayer and fewlayer MoS_2 films onto arbitrary substrates. *ACS Nano* **2014**, *8*, 11522–11528.

[51] Feng, Q. L.; Zhu, Y. M.; Hong, J. H.; Zhang, M.; Duan, W. J.; Mao, N. N.; Wu, J. X.; Xu, H.; Dong, F. L.; Lin, F. et al. Growth of large-area 2D $MoS_{2(1-x)}Se_{2x}$ semiconductor alloys. *Adv. Mater.* **2014**, *26*, 2648–2653.

[52] Lee, C.; Yan, H. G.; Brus, L. E.; Heinz, T. F.; Hone, J.; Ryu, S. Anomalous lattice vibrations of single- and few-layer MoS_2. *ACS Nano* **2010**, *4*, 2695–2700.

[53] Zhang, Y.; Zhang, Y. F.; Ji, Q. Q.; Ju, J.; Yuan, H. T.; Shi, J. P.; Gao, T.; Ma, D. L.; Liu, M. X.; Chen, Y. B. et al. Controlled growth of high-quality monolayer WS_2 layers on sapphire and imaging its grain boundary. *ACS Nano* **2013**, *7*, 8963–8971.

[54] Hsu, W.-T.; Zhao, Z.-A.; Li, L.-J.; Chen, C.-H.; Chiu, M.-H.; Chang, P.-S.; Chou, Y.-C.; Chang, W.-H. Second harmonic generation from artificially stacked transition metal dichalcogenide twisted bilayers. *ACS Nano* **2014**, *8*, 2951–2958.

[55] Liu, C.-H.; Chang, Y.-C.; Norris, T. B.; Zhong, Z. H. Graphene photodetectors with ultra-broadband and high responsivity at room temperature. *Nat. Nanotechnol.* **2014**, *9*, 273–278.